Am J Physiol Heart Circ Physiol 285: H183–H193, 2003.
First published February 21, 2003; 10.1152/ajpheart.00490.2002.

Mechanisms of Arg-Pro-Pro-Gly-Phe inhibition of thrombin

Ahmed A. K. Hasan,[1,2] Mark Warnock,[2] Marvin Nieman,[2] Sujata Srikanth,[1] Fakhri Mahdi,[1] Raman Krishnan,[3] Alexander Tulinsky,[3] and Alvin H. Schmaier[1,2]

[1]*Division of Hematology and Oncology, Department of Internal Medicine, University of Michigan, Ann Arbor 48109-0640;* [2]*Thromgen, Incorporated, Ann Arbor 48104; and*
[3]*Department of Chemistry, Michigan State University, East Lansing, Michigan 48824*

Submitted 11 June 2002; accepted in final form 3 February 2003

Hasan, Ahmed A. K., Mark Warnock, Marvin Nieman, Sujata Srikanth, Fakhri Mahdi, Raman Krishnan, Alexander Tulinsky, and Alvin H. Schmaier. Mechanisms of Arg-Pro-Pro-Gly-Phe inhibition of thrombin. *Am J Physiol Heart Circ Physiol* 285: H183–H193, 2003. First published February 21, 2003; 10.1152/ajpheart.00490.2002.—Investigations determined the mechanism(s) by which Arg-Pro-Pro-Gly-Phe (RPPGF) inhibits thrombin-induced platelet activation. High concentrations of RPPGF inhibit thrombin-induced coagulant activity. RPPGF binds to the active site of thrombin by forming a parallel β-strand with Ser^{214}-Gly^{216} and interacts with His^{57}, Asp^{189}, and Ser^{195} of the catalytic triad. RPPGF competitively inhibits α-thrombin from hydrolyzing Sar-Pro-Arg-paranitroanilide with a $K_i = 1.75 \pm 0.03$ mM. Other mechanisms were sought to explain why RPPGF inhibits thrombin activation of platelets at concentrations below that which inhibits its active site. Soluble RPPGF blocks biotinylated NATLDPRSFLLR of the thrombin cleavage site on protease-activated receptor (PAR)1 from binding to the peptide RPPGC (IC_{50} = 20 μM). The soluble recombinant extracellular domain of PAR1 ($rPAR1_{EC}$) blocks biotinylated RPPGF binding to $rPAR1_{EC}$ (IC_{50} = 50 μM) bound to microtiter plates, but $rPAR1_{EC}$ deletion mutants missing the sequence LDPR or PRSF do not. RPPGF and related forms prevent the thrombin-like enzyme thrombocytin from proteolyzing $rPAR1_{EC}$ at concentrations that do not block thrombocytin's active site. These studies indicate that RPPGF is a bifunctional inhibitor of thrombin: it binds to PAR1 to prevent thrombin cleavage at Arg^{41} and interacts with the active site of α-thrombin.

protease-activated receptor 1; bradykinin-(1–5); thrombin inhibitor; thrombin receptor

INVESTIGATIONS SHOW THAT the angiotensin-converting enzyme breakdown product of bradykinin, Arg-Pro-Pro-Gly-Phe (RPPGF), is a stable metabolite of bradykinin (11, 16). Infusion of RPPGF in vivo protects against the deleterious effects of lipopolysaccharide, suggesting that this peptide has biological activity (15). We have shown that RPPGF is an inhibitor of α-thrombin-induced platelet activation (3). RPPGF and related compounds inhibit both α- and γ-thrombin-induced platelet aggregation and secretion without inhibiting ADP-, collagen-, or U-46619-induced platelet activation (3). RPPGF does not inhibit thrombin binding to platelets, SFLLRN-induced platelet activation, or α-thrombin cleavage of H-D-Phe-Pip-Arg-paranitroanilide (3). It directly binds to the platelet membrane (5). RPPGF prevents α-thrombin from cleaving the peptide NATLDPRSFLLR, which spans the thrombin cleavage site on protease-activated receptor 1 (PAR1), between Arg and Ser (3).

The importance of RPPGF and related compounds has been shown in animal studies (5, 6). High concentrations of RPPGF are as effective as aspirin in preventing electrolytic injury-induced left circumflex coronary artery thrombosis in dogs (5). Combined RPPGF and aspirin result in a summating antithrombotic effect (5). In the Folts canine model for induced cyclic flow variations, a multiantigenic peptide (MAP) form of RPPGF, MAP4-RPPGF, significantly reduced cyclic flow variations similar to aspirin or clopidogrel (6). In an ex vivo model of balloon angioplasty injury to the vessel wall, RPPGF was as effective as aspirin in preventing platelet adherence to the vessel wall and fibrin formation (20). The present investigation characterizes the mechanism(s) of RPPGF inhibition of thrombin. RPPGF inhibits thrombin activation of platelets in two ways. It directly binds to the active site of thrombin, and it binds to the extracellular domain of PAR1 to prevent thrombin cleavage after Arg^{41}.

MATERIALS AND METHODS

Proteins. Human α-thrombin (3,250 or 3,000 U/mg), γ-thrombin, and hirudin were purchased from Hematologic Technologies (Essex Junction, VT). Bovine serum albumin was purchased from Sigma (St. Louis, MO). Thrombocytin was a generous gift from the late S. Niewiarowski, Temple University (Philadelphia, PA).

Peptides. Peptides RPPGF, RPPGC, MAP4-RPPGF, FPRPG, GPRP, and NATLDPRSFLLR (NAT12) were synthesized by the Protein and Carbohydrate Structure Facility, University of Michigan (Ann Arbor, MI), and at Multiple Peptide System (San Diego, CA). MAP4-RPPGF is a multiantigenic form of RPPGF consisting of a β-Ala core with an attached Lys followed by two attached Lys and four molecules of RPPGF attached to the two latter Lys (6). Each peptide was made with the COOH-terminal amino acid covalently attached to a solid phase support, and succeeding amino acids were coupled sequentially to the NH_2 terminus (4, 6). Additional peptides, biotinylated RPPGF (biotin-RP-

Address for reprint requests and other correspondence: A. H. Schmaier, Univ. of Michigan, 5301 MSRB III, 1150 W. Medical Center Dr., Ann Arbor, MI 48109-0640 (E-mail: aschmaie@umich.edu).

The costs of publication of this article were defrayed in part by the payment of page charges. The article must therefore be hereby marked "*advertisement*" in accordance with 18 U.S.C. Section 1734 solely to indicate this fact.

PGF) and biotinylated NATLDPRSFLLR-amide (biotin-NAT12), were synthesized at Quality Controlled Biochemical (Hopkinton, MA) and at Multiple Peptide System. All peptides were purified by preparative reverse-phase HPLC and characterized by analytic HPLC, amino acid analysis, and mass spectrometry. Each peptide was colorless, odorless, and soluble in water. Each peptide is described using the single capital letter designation for each L-amino acid. Some longer peptides are named by the single letter code for their first three amino acids, followed by the total number of amino acids in the peptide.

Antibodies. Polyclonal antibodies to the thrombin cleavage sites on its three cell receptors were raised in goats at Quality Controlled Biochemical, by immunizing with peptides ^{35}NATLDPRSFLLRN^{47}, ^{35}KPTLPIKTFRGAP^{47}, or ^{41}SILPAPRGYPGQV^{53} from the extracellular domain of human PAR1, PAR3, or PAR4, respectively. The numbering listed for these peptides here and elsewhere is that of the amino acid sequence on the extracellular domains of each of these human PARs (8, 27, 28). Each anti-PAR antibody was purified on affinity chromatography by coupling each peptide to AfFigel-15, Bio-Rad (Richmond, CA) in dimethyl sulfoxide. Anti-His_6 monoclonal antibody (His-tag monoclonal antibody) was purchased from Novagen (Madison, WI). Monoclonal antibodies SPAN12 and WEDE15 were obtained from Immunotech, a subsidiary of Coulter (Miami, FL). SPAN12 was raised against peptide ^{35}NATLDPRSFLLR^{46}, and WEDE15 was raised against peptide ^{51}KYEPFWEDEEKNES^{64}, the hirudin-like domain on PAR1 (14).

Other materials. Full-length cDNA to human PAR1 was kindly provided by Dr. Lawrence Brass, University of Pennsylvania (Philadelphia, PA). A bacterial expression system with the pET19b vector was purchased from Novagen; fura 2-AM was obtained from Molecular Probes (Eugene, OR). Hirugen [sulfated acyl-hirudin$_{53-65}$, *N*-acetyl-NGDFEEIPEEY (SO_3) LQ] was obtained from Bachem Bioscience (King of Prussia, PA). Rabbit thrombomodulin (TM) was purchased from American Diagnostica (Greenwich, CT).

Ability of RPPGF to inhibit the coagulant activity of α-thrombin. The ability of RPPGF to inhibit the activated partial thromboplastin time (APTT), prothrombin time (PT), or thrombin clotting time (TCT) was investigated. The APTT and PT were performed as previously reported in the absence or presence of 0.03125–3 mM RPPGF (5, 6). The TCT experiments were performed by incubating 100 μl of pooled normal human plasma (George King; Overland Park, KS) in the absence or presence of 0.03125–3 mM RPPGF at 37°C for 5 min. At the end of incubation, 8 nM human α-thrombin (1 U/ml) was added, and the time to clot formation was measured. All the coagulant assays were performed in a Amelung KC4 coagulation meter (Sigma). In other experiments, normal human plasma was made to 3 mM with L-Arg, and the APTT, PT, or TCT was measured.

Crystal structure of the human α-thrombin-thrombostatin complex. Investigations were performed to determine whether RPPGF directly interacted with α-thrombin. A thrombin-hirugen complex was prepared with human α-thrombin (Enzyme Research Laboratories; South Bend, IN). The thrombin-hirugen complex was made by adding 10-fold molar excess hirugen to a solution of 1 mg/ml α-thrombin in 750 mM NaCl and 0.1 M sodium phosphate buffer (pH 7.3). Independently, peptide NAT12 was added to RPPGF in a 1:1 molar ratio to form a complex (25 mg/ml in water). Each complex, thrombin-hirugen and NAT12-RPPGF, was left overnight at 4°C to complete complexation. The thrombin-hirugen complex then was concentrated to 4 mg/ml. Ten-fold molar excess NAT12-RPPGF complex was then added to the concentrated thrombin-hirugen complex. The resultant presumed quaternary complex was left to stand for a day before the crystallization was set up. Crystal Screen 1 (Hampton Research; Laguna Hills, CA) was used to scan the initial conditions. Small crystals were obtained from *factorials 20* and *31*, both of which had PEG 4000 as the precipitant. Crystals suitable for X-ray diffraction were grown in 23.5% PEG 4000 and 0.1 M sodium acetate (pH 4.6) containing 0.2 M ammonium sulphate. A crystal of $0.2 \times 0.2 \times 0.15$ mm was used for collecting the diffraction data, which diffracted X-rays to a resolution of 2.1 Å.

Intensity data were measured with a R-AXIS II imaging plate detector equipped with Molecular Structure focusing mirrors using CuK radiation from a Rigaku RU200 rotating anode generator operating at 5 kW power with a fine focus filament (0.3×3.0 mm). The crystal to detector distance was 102 mm, and each frame was collected for 15 min with an oscillation of 2.5°. The total scan range for the data collection was 125°, and the total exposure time was <15 h. The unit cell was determined by autoindexing (7), and the processing of the raw data was carried out with the Rigaku R-AXIS data-processing software package. The crystals were orthorhombic: unit cell dimensions of $a = 79.15$ Å, $b = 104.97$ Å, and $c = 45.18$ Å, belonging to the space group $P2_12_12$. Of a total of 23,504 independent measurements, 17,158 measurements corresponded to $I/\Sigma(I) > 1.5$, where I is the intensity of the reflections (73%, $R_{merge} = 0.068$). This data set is 78% complete for a resolution of 2.5 Å and contains one-half the reflections for a resolution between 2.3 and 2.1 Å.

The orientation of the thrombin molecule in the crystal was determined using Patterson search techniques as implemented in the program AMoRe (17). The thrombin coordinates used for the molecular replacement calculations were of the CVS995-thrombin complex (entry 1DIT, Brookhaven Protein Data Bank) stripped of solvent and the inhibitor molecule (10). The cross-rotation search was conducted at two resolution ranges, 8.0–3.5 and 10.0–3.5 Å, which had a unique solution of 7 σ above the mean. A translational search performed in the space group $P2_12_12$ also gave an outstanding solution (correlation of 0.62, $R = 37\%$). The starting model was refined using restrained least-squares methods with the program PROFFT (2). The modeling and electron density fitting was carried out on a Silicon Graphics Indigo workstation using the program CHAIN (21). After 15 cycles of overall B refinement (temperature factor or B factor) at a resolution of 2.8 Å, the *R* factor converged to 29%. Individual B refinement reduced the *R* factor further to 25%. Different electron density maps were analyzed to find hirugen and the bound peptide. The structure was then refined using standard techniques, including solvent, to a final *R* factor of 20.2% with 105 solvent water molecules (12). The average thermal factors for the protein and water molecules were 24.6 and 25.7 Å^2, respectively.

Ability of RPPGF to directly inhibit the enzymatic activity of α-thrombin. Investigations were performed to determine whether the enzymatic activity of α-thrombin could be directly inhibited by RPPGF. Initial studies determined the K_m of α-thrombin for the chromogenic substrates H-D-Phe-Pip-Arg-paranitroanilide (S2238, DiaPharma; Franklin, OH) and Sar-Pro-Arg-paranitroanilide (Sigma) in 0.01 M Tris and 0.15 M NaCl (pH 7.6). Additional studies were performed to determine whether 0.125–2 mM RPPGF would interfere with the ability of α-thrombin (1.25 nM) to hydrolyze 0.7 mM S2238 or 0.6 mM Sar-Pro-Arg-paranitroanilide in 0.01 M Tris and 0.15 M NaCl (pH 7.6). Further studies were performed to determine the nature of the inhibition of α-thrombin (1.25 nM) by 0.125–2 mM RPPGF to hydrolyze Sar-Pro-Arg-para-

nitroanilide. In these experiments, increasing concentrations of RPPGF (0–2 mM) were incubated with 1.25 nM α-thrombin in the presence of 0.04–0.5 mM Sar-Pro-Arg-paranitroanilide at 37°C for 1 h. The rate of substrate hydrolysis over 1 h was monitored at 37°C. Preliminary experiments revealed that the hydrolysis of this substrate by α-thrombin (1.25 nM) under these conditions was linear for over 1 h. The data in the absence or presence of RPPGF were plotted on a Lineweaver-Burk reciprocal plot of $1/V$ vs. 1/[S], where $1/V$ is the maximal velocity and [S] is the concentration of the substrate. The K_i of RPPGF inhibition of α-thrombin was determined by two methods: a plot of the negative x-intercept reciprocal (apparent K_m) or the slope of the reciprocal plot at each inhibitor concentration versus the inhibitor concentration (23). Both methods were used to verify the determination of the K_i of the interaction.

Additional investigations determined whether the weak inhibitory activity of RPPGF on the enzymatic activity of α-thrombin could be modulated by occupancy of exosite 1 by TM or sulfated *N*-acetyl hirudin$_{53–64}$ (26). In these experiments, 1.25 nM α-thrombin was mixed with either 2 nM TM or 1 μM hirugen in 20 mM Tris acetate, 140 mM NaCl, 5 mM KCl, 1 mM $MgCl_2$, and 1 mM $CaCl_2$ (pH 7.5) and incubated at room temperature for 6–15 min before addition to the assay. The incubation mixtures were then added to Sar-Pro-Arg-paranitroanilide (0.5 mM in 0.01 M Tris and 0.15 M NaCl; pH 7.6) in the absence (control) or presence of increasing concentrations of RPPGF (0–3 mM), followed by further incubation at 37°C for 1 h. The hydrolysis of the substrate over 1 h was determined by monitoring the absorbance at 405 nm. The change in the rate of substrate hydrolysis over 1 h in the samples containing various concentrations of RPPGF was compared with samples that did not contain the peptide.

Cloning and expression of the extracellular fragment of human PAR1. A portion of the extracellular domain of human PAR1 (Ala^{26}-Ser^{99}) ($rPAR1_{EC}$) was expressed in *Escherichia coli* using a bacterial expression system (Novagen) and its pET19b vector. Oligonucleotide primers for PCR were designed to place *Nde*I and *Xho*I restriction sites at the 5′ and 3′ ends of the coding sequence, respectively. PCR using human PAR1 cDNA as the template prepared human PAR1 DNA encoding residues Ala^{26}-Ser^{99}. The *Nde*I-*Xho*I PCR fragment was ligated to the *Nde*I/*Xho*I sites of pET19b to create pET19b/$PAR1_{EC}$. This plasmid was then used to transform NovaBlue, an *E. coli* K12 strain. The insert of the cloned DNA was sequenced, and it showed 100% fidelity with the DNA sequence of the targeted NH_2-terminal extracellular domain of PAR1. The His_{10}-DDDDK-$PAR1_{EC}$ fusion construct was produced in *E. coli* strain BL21(DE3) by transforming with pET19b/$PAR1_{EC}$ and inducing it with 1 mM isopropyl-β-D-thiogalactopyranoside (IPTG) for 2 h. The expressed $rPAR1_{EC}$ (Ala^{26}-Ser^{99}) fusion protein was purified from bacterial cytosolic fractions by nickel-chelate affinity chromatography (HisTrap Affinity Column, Amersham Pharmacia Biotech; Piscataway, NJ). The bound recombinant protein was eluted with 20 mM phosphate, 0.5 M NaCl, and 500 mM imidazole (pH 7.4), dialyzed into 0.01 M Tris and 0.15 M NaCl (pH 8), and stored in aliquots at −70°C. Recombinant $PAR1_{EC}$ was characterized by 16.5% Tris-tricine SDS-PAGE, NH_2-terminal sequencing, immunoblotting with anti-PAR1 antibodies, and cleavage experiments using thrombin or thrombocytin (see RESULTS).

Site-directed mutagenesis. The pET19b/$PAR1_{EC}$ plasmid was used to express several deletion mutants (*mutants I–V* and *VII*) of $rPAR1_{EC}$ (Table 1). Oligonucleotide-directed mutagenesis using the GeneEditor mutagenesis kit (Promega; Madison, WI) was performed to generate the mutants of $rPAR1_{EC}$ in the expression vector pET19b/$PAR1_{EC}$. Briefly, mutants were selected based on the incorporation of a second site mutation in β-lactamase, which alters its substrate specificity, allowing resistance in transformed bacteria to cefotaxime and ceftriaxone in addition to ampicillin. Incorporation of the deletion was verified by DNA sequencing. The mutagenesis primers for the introduction of site-directed deletion were as follows: *mutant I* primer, 5′-GCAACAAATGCCACCCCCCGGTCATTTCTTC-3′; *mutant II* primer, 5′-AATGCCACCTTAGATTCATTTCTTCTCAGG-3′; *mutant III* primer, 5′-GCCACCTTAGATCCCTTTCTTCTCAGGAAC-3′; *mutant IV* primer, 5′-GCAACA AATGCCACCTCATTTCTTCTCAGG-3′; *mutant V* primer, 5′-AATGCCACCTTAGATCTTCTCAGGA-ACCCC-3′; and *mutant VII* primer, 5′-ACCCCCAATGATAAAGAGGATGAGGAGAAAAATG-3′. Plasmid DNA was prepared using reagents supplied by Qiagen (Valencia, CA), and recombinant site-directed deletion mutants of the extracellular domain of human PAR1 were expressed in *E. coli* strain BL21(DE3) after induction with 1 mM IPTG. The expressed mutant proteins were purified from bacterial cytosol by nickel-chelate affinity chromatography as described above.

Table 1. *Interactions of RPPGF in the active site of α-thrombin*

RPPGF Amino Acids	α-Thrombin	
	Amino acids	Distance, Å
Arg^1 N	Wat^{601} O	2.9
Arg^1 N	His^{57} NE	3.1
Arg^1 N	Ser^{195} OG	2.4
Arg^1 N	Ser^{214} O	3.0*
Arg^1 NE	Wat^{508} O	2.7
Arg^1 NH1	Asp^{189} OD1	2.9
Arg^1 NH2	Asp^{189} OD2	3.0
Arg^1 NH2	Gly^{216} O	2.9
Arg^1 NH2	Wat^{508} O	2.9
Arg^1 O	Wat^{550} O	2.8
Pro^2 CD	His^{57} CE1	3.2
Pro^2 CG	Trp^{60D} CH2	3.3
Pro2 O	Trp^{215} CB	2.8
Pro^2 O	Gly^{216} N	3.3*
Pro^3 N	Gly^{216} O	3.3

The peptide Arg-Pro-Pro-Gly-Phe (RPPGF) is numbered 1–4 beginning with Arg. α-Thrombin is numbered using a topological equivalence in tertiary structure to chymotrypsin (1). *Poor hydrogen bonding angle (~90°C).

Examining the interaction of RPPGF with PAR1. Peptide RPPGC at 5–10 μg/well in 0.1 M Na_2CO_3 (pH 9.6) was bound to microtiter plate wells (F96 CERT.MAXISORP, No. 439454, Nunc-Immuno Plate, Fisher Scientific; Chicago, IL) by overnight incubation at 4°C or for 2 h at 37°C. In preliminary experiments, it was found that more biotin-NAT12 bound to cuvette wells linked with the peptide RPPGC than with RPPGF. Presumably, the COOH-terminal Cys on RPPGC allowed for more of it to adsorb to microtiter plates than RPPGF. After incubation, the contents of the wells were discarded, and the wells were washed with 0.01 M Na_2PO_4 and 0.15 M NaCl (pH 7.4) containing 0.01% Tween 20 (PBS-Tween). After each well was blocked with 1% radioimmunoassay grade bovine serum albumin, the bound peptides were incubated with 30 μM biotin-NAT12 in the absence or presence of increasing concentrations of RPPGF, NAT12, or scrambled peptides for 1 h at 37°C. Detection of bound biotinylated peptide was performed by using Immuno-Pure streptavidin horseradish peroxidase conjugate from Pierce

Chemical (Rockville, IL) and peroxidase-specific fast reacting substrate turbo-3,3′,5,5′-tetramethylbenzidine (turbo-TMB, Pierce) as previously described (4). The color reaction was stopped by the addition of 1 M phosphoric acid, and the bound biotinylated peptide had its absorbance measured at 450 nm using a Microplate auto reader EL311 (Bio-Tek; Winooski, VT).

In other binding experiments, purified $rPAR1_{EC}$ (1 μg/well) was coupled to microtiter plates as described above. After each well was blocked, 1 mM RPPGF was incubated with the microtiter plate cuvette wells. Detection of the bound RPPGF was performed using a polyclonal rabbit antibody to RPPGF (Dainippon Pharmaceutical; Osaka, Japan), followed by the addition of a goat anti-rabbit antibody conjugated with horseradish peroxidase (Sigma). The antibody to RPPGF was specific to this peptide and did not recognize bradykinin, RPPGFSPFR (data not shown). After incubation, the enzyme conjugate on the cuvette well was measured by peroxidase-specific fast reacting substrate turbo-TMB (Pierce), as described above (4).

Additional experiments determined whether soluble $rPAR1_{EC}$ or the six deletion mutants blocked biotin-RPPGF binding to $rPAR1_{EC}$ coupled to cuvette wells. In these experiments, $rPAR1_{EC}$ at 1 μg/well was linked to microtiter plate cuvette wells in 0.1 M Na_2CO_3 (pH 9.6) by overnight incubation at 4°C. After it was linked, 10 μM biotin-RPPGF was incubated with the cuvette wells in the absence or presence of increasing concentrations of $rPAR1_{EC}$, its deletion mutants, or 5 mM L-Arg (Sigma). The amount of biotin-RPPGF bound was determined as described above (4).

Digestion of $rPAR1_{EC}$ by proteolytic enzymes in the absence or presence of RPPGF or MAP4-RPPGF. $rPAR1_{EC}$ (1 μg) in 0.01 mM Tris·HCl and 0.2 M NaCl (pH 8.0) was incubated at 37°C for 15 or 45 min with 1 nM α-thrombin or 0.5 μg/ml (16.7 nM) thrombocytin, respectively, in the absence or presence of 0.125–1 mM RPPGF or 0.05–0.5 mM MAP4-RPPGF. The reaction mixture was separated by SDS-PAGE and stained with Coomassie Brilliant blue. The cleaved gel images were scanned using Scion Image software (ScionCorp; Frederick, MD).

Ability of RPPGF to directly inhibit the enzymatic activity of thrombocytin. Studies determined whether 0.5–2 mM of RPPGF or 0.2–1 mM MAP4-RPPGF interfered with the ability of 0.5 μg/ml thrombocytin (16.7 nM) to hydrolyze 1.0 mM H-D-Phe-Pip-Arg-paranitroanilide in 0.01 M Tris and 0.15 M NaCl (pH 7.6) buffer. The initial rate of hydrolysis of the substrate was determined by monitoring absorbance at 405 nm over 30 min.

RESULTS

Direct interaction of RPPGF with human α-thrombin. Investigations were performed to determine the mechanism(s) by which RPPGF inhibited thrombin-induced platelet aggregation. Initial studies determined whether RPPGF inhibited the coagulant activity of thrombin (Fig. 1). As the concentration of RPPGF increased from 0.031 to 3 mM, there was a significant prolongation of the TCT at ≥0.125 mM ($P < 0.01$), the APTT at ≥0.25 mM ($P < 0.016$), and the PT at ≥0.5 mM ($P < 0.003$). At the 0.5 mM concentration of RPPGF, the TCT or APTT was more significantly prolonged ($P < 0.0005$ and $P < 0.001$ levels, respectively) than the PT. The increased sensitivity of inhibition of the APTT over the PT may have arisen from the fact that RPPGF inhibits factor XI activation (6). Because

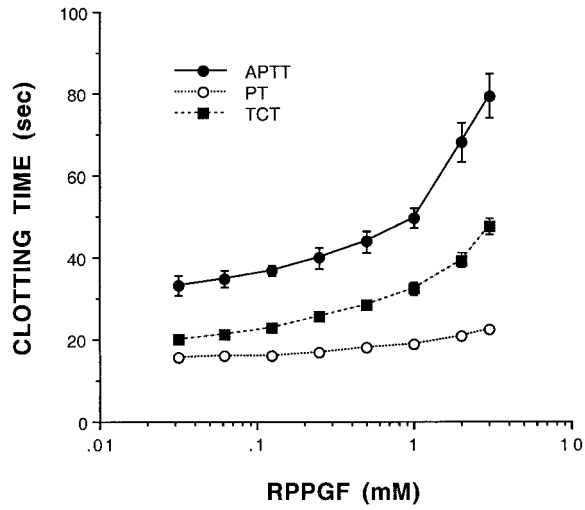

Fig. 1. Influence of Arg-Pro-Pro-Gly-Phe (RPPGF) on coagulant assays. Pooled normal human plasma was made to 0.03125–3 mM with RPPGF. The treated plasma was assayed for the effect of RPPGF on the clotting time (in s) of the activated partial thromboplastin time (APTT), prothrombin time (PT), or thrombin clotting time (TCT). Data are means ± SD of 6 experiments performed on 6 different days.

RPPGF had a direct interaction with thrombin, studies were performed to determine whether L-Arg itself influenced these assays. L-Arg at a final concentration of 3 mM did not prolong any of the coagulant assays. These data indicate that the effect of RPPGF on the coagulant assays was specific for this peptide and not its NH_2-terminal Arg.

Investigations to determine whether there is evidence for a physical interaction between RPPGF and thrombin. Studies were then performed to determine whether RPPGF interacts with preformed α-thrombin crystals. A preformed NAT12-RPPGF complex was incubated with an α-thrombin-hirugen crystal. Examination of its electron density map revealed the presence of residues RPPG of RPPGF bound in the active site, in a retro manner, i.e., the NH_2-terminal arginine is in the active site (Fig. 2), with hirugen bound at exosite I (Fig. 3) (21, 22). However, even though a solution of RPPGF and NAT12 was used for cocrystallization with hirugen-thrombin, electron density maps only revealed RPPG interacting with the thrombin active site and did not reveal any bound NAT12 or parts thereof in the crystal structure (Figs. 2–4).

The interaction of RPPGF with the active site of α-thrombin is shown in Fig. 4. RPPGF was a retro-binder to the active site of α-thrombin because its NH_2 terminal fitted into the specificity (S1) pocket and the main chain ran parallel (from the NH_2 to COOH terminal) with respect to Ser^{214}-Gly^{216} (13, 19). In normal substrate binding, the main chain of the peptide runs from the COOH to NH_2 terminal. The location of the Arg of RPPG, being inserted in the S1 pocket, was clearly evident in fitting the peptide to the electron density map (Fig. 2). With the NH_2-terminal Arg in the S1 pocket, the Pro residues were unambiguously assigned positions, one occupying the S2 site (Figs. 2 and

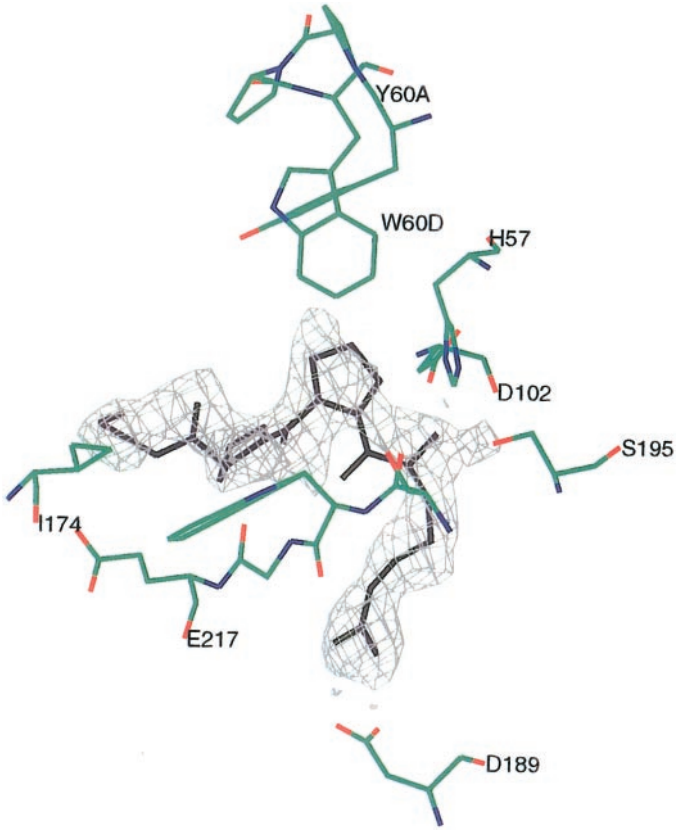

Fig. 2. Final ($2F_0$-F_0) electron density of RPPG in the active site of human α-thrombin. Contoured at the 1 σ-level. RPPG, black; thrombin atom colors: carbon, green; nitrogen, blue; oxygen, red. The two Pro residues of RPPG restrain the peptide from assuming the good hydrogen bonds of a parallel β-strand. The amino acid numbering shown is that of thrombin (1).

Fig. 3. RPPG and hirugen bound to thrombin. Schematic representation of the location of RPPG and hirugen on human α-thrombin. RPPG is retrobound to the active site; hirugen is bound to exosite I of thrombin. The red cylinders represent α-helixes; the yellow ribbons represent β-sheets.

4). This Pro interacted with His^{57}, Trp^{60D}, Trp^{215}, and Gly^{216} (Table 1). The two adjacent Pro limit the conformation of RPPG, preventing it from forming good hydrogen bonding interactions of a parallel β-strand.

The NH_2-terminal arginyl is located in the S1 pocket of the active site (Fig. 4). It interacted with His^{57}, Asp^{189}, Ser^{195}, and Ser^{214} (Table 1). The binding orientation of RPPG is unusual because the main chain direction is opposite to the main chain direction of thrombin substrates. There are generally two hydrogen bonds from substrate/inhibitor to the Gly^{216} backbone oxygen and nitrogen atoms. In the present structure, however, only one longer hydrogen bond is observed. The presence of Arg in the specificity pocket allowed for all the expected interactions with the surrounding molecules, including the water-mediated interactions of the NE atom with Gly^{216} (Table 1). The arginyl side chain atoms have lower thermal factors compared with the remainder of RPPGF, suggesting better binding in the specificity S1 pocket. The final coordinates of the ternary complex have been deposited in the Protein Data Bank (code 1NY2).

Ability of RPPGF to directly inhibit the enzymatic activity of α-thrombin. Because RPPGF physically interacted with the active site of α-thrombin, investigations determined whether RPPGF interfered with the

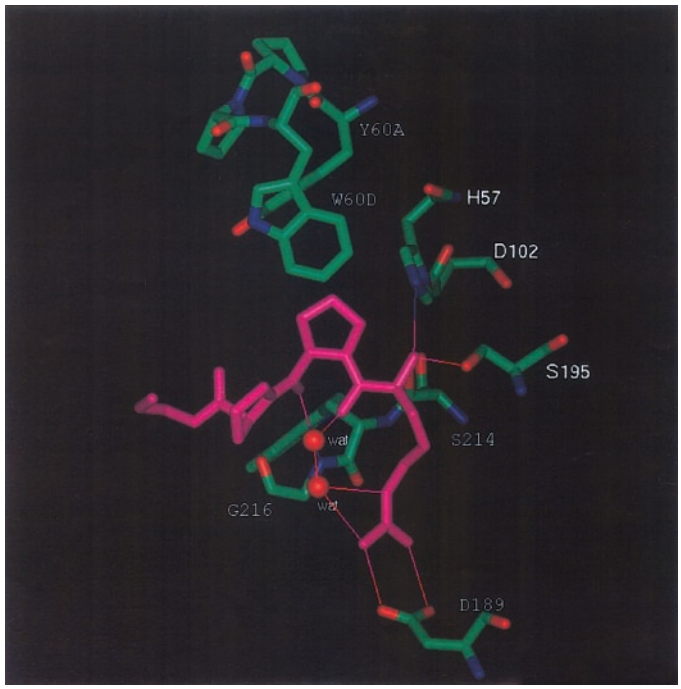

Fig. 4. RPPG interactions with the active site of α-thrombin. The peptide RPPG (violet) is retrobound to the active site with the NH_2-terminal Arg of RPPG interacting with the S1 pocket (see Table 1 for a complete listing of interactions). The hydrogen bonds are thin violet-orange-colored lines. The amino acid numbering shown is that of thrombin (1).

enzymatic activity of α-thrombin. Previous studies using the chromogenic substrate H-D-Phe-Pip-Arg-paranitroanilide showed that RPPGF did not interfere with the ability of α-thrombin to hydrolyze that substrate (11). The K_m for α-thrombin to hydrolyze H-D-Phe-Pip-Arg-paranitroanilide was 6 μM in 0.01 M Tris and 0.15 M NaCl at pH 8.3 and 37 μM in the same buffer at pH 7.6 (26). Because RPPGF at only 332–680 μM inhibited α-thrombin's ability to activate human platelets, α-thrombin had a higher affinity to the chromogenic substrate H-D-Phe-Pip-Arg-paranitroanilide substrate than to RPPGF (3, 5, 6). However, using an α-thrombin substrate, Sar-Pro-Arg-paranitroanilide, which has a lower K_m (138 μM), progressive inhibition of α-thrombin's ability to hydrolyze the substrate was seen when the RPPGF concentration was >1 mM (data not shown). At 2 mM RPPGF, there was 50% inhibition of α-thrombin-induced hydrolysis of Sar-Pro-Arg-paranitroanilide. Alternatively, RPPGF was unable to inhibit α-thrombin's ability to hydrolyze H-D-Phe-Pip-Arg-paranitroanilide at concentrations up to 3 mM, as previously reported (data not shown) (3). These data suggest that RPPGF interacted weakly with the active site of α-thrombin to inhibit thrombin's amidolytic activity.

Investigations were then performed to determine the kinetics of RPPGF inhibition of α-thrombin (Fig. 5). With the use of Sar-Pro-Arg-paranitroanilide concentrations around the K_m of α-thrombin hydrolysis, there was a progressive increase in the apparent K_m as the concentration of RPPGF increased in the reaction mixture (23). On reciprocal plot 1/*V* versus 1/[S], the maximal velocity of each reaction, 1/*V*, was approximately the same in the absence or presence of increasing concentrations of RPPGF (0.125–2.0 mM). Similarly, on the reciprocal plot, there was a progressive increase in the K_m (Fig. 5). The results of this experiment indicated competitive inhibition, consistent with RPPGF interacting with the active site of α-thrombin (23). The K_i of RPPGF inhibiting α-thrombin from hydrolyzing this substrate was 1.75 ± 0.03 mM. Additional investigations were performed to determine whether occupancy of thrombin's exosite I altered RPPGF's ability to inhibit thrombin. Thrombomodulin or sulfated *N*-acetyl hirugen$_{53–64}$ did not alter the ability of RPPGF to inhibit thrombin (data not shown). These latter data indicated that the interaction of RPPGF with the active site of the thrombin-hirugen complex is representative of the interaction of RPPGF with free thrombin and is not modified by proteins or peptides occupying thrombin's exosite I.

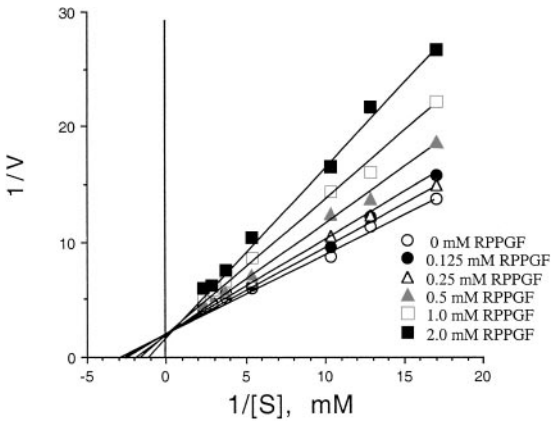

Fig. 5. Ability of RPPGF to directly inhibit the proteolytic activity of human α-thrombin. A reciprocal plot of the maximal velocity (1/*V*) versus the concentration of the substrate (1/[S]) was performed on the results of α-thrombin (1.25 nM) hydrolyzing the substrate Sar-Pro-Arg-paranitroanilide (0.04–0.5 mM) in the absence or presence of 0.125–2.0 mM RPPGF. Values shown are means of 3 independent experiments.

Interaction between RPPGF and a peptide that includes the thrombin cleavage site on the extracellular fragment of PAR1. The above studies indicated that RPPGF was a weak, active site binding inhibitor of thrombin. This interpretation of the mechanism by which RPPGF inhibits thrombin activation of platelets, however, did not completely correlate with some previous in vitro and in vivo studies (5). FITC-labeled RPPGF binds to platelets, and thrombin inhibition by RPPGF of canine platelets in vivo was present 150 min after no RPPGF (i.e., <1 μM) could be measured in plasma. These latter data suggested that RPPGF may prevent thrombin activation of platelets by another mechanism than just active site thrombin inhibition as described above. Investigations were performed to determine whether there is a physical interaction between RPPGF and thrombin's major receptor on platelets, PAR1.

Initial studies determined whether there were any interaction between RPPGF and a peptide (NAT12) that included the thrombin cleavage site on the extracellular domain of human PAR1. Preliminary investigations showed that biotin-NAT12 did not bind nonspecifically to microtiter plate wells, albumin, or irrelevant peptides (data not shown). When peptide RPPGC, a peptide that binds plastic more avidly, was coupled to microtiter plates, RPPGF blocked biotin-NAT12 peptide binding with an IC_{50} of 20 μM (Fig. 6). Unlabeled peptide NAT12 also blocked biotin-NAT12 binding with an IC_{50} of 500 μM. Alternatively, two scrambled peptides of RPPGF, FPRPG or GPRP, did not block biotin-NAT12 binding (Fig. 6). These experiments suggest that there might be a physical interaction between RPPGF and the thrombin cleavage site on the extracellular domain of PAR1.

Preparation and characterization of the extracellular domain of human PAR1. To further examine whether there is an interaction between RPPGF and the extracellular domain of PAR1, a recombinant form of a portion of the extracellular domain of PAR1 (rPAR1$_{EC}$) was prepared. With the use of pET19b/PAR1$_{EC}$, a fusion protein was produced at 11 kDa, as seen on Coomassie-stained Tris-tricine SDS-PAGE gels, respectively (see Fig. 10, rPAR1 lane). On amino acid sequencing, the rPAR1$_{EC}$ protein produced by pET19b had complete amino acid identity with native human PAR1 from amino acids 26–99 (data not shown). The recombinant extracellular domain of human PAR1 was recognized by a goat polyclonal antibody to PAR1 or monoclonal antibody SPAN12, both raised to a peptide

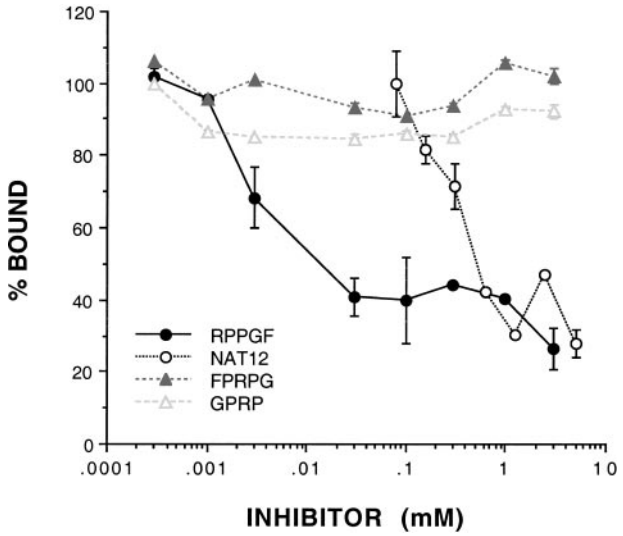

Fig. 6. Ability of RPPGF to compete biotinylated (biotin-)NAT12 binding to RPPGC. The peptide RPPGC (5 μg/well) was linked to microtiter plate wells in 0.1 M Na_2CO_3 (pH 9.6) overnight at 4°C. After the wells were washed and blocked with 1% bovine serum albumin, 0.03 mM biotin-NAT12 was added in the presence of increasing concentrations of RPPGF, NAT12, FPRPG, or GPRP. %Bound represents the percentage of the level of binding seen in the presence of a competitor versus that seen in the absence of the competitor. The amount of bound biotin-NAT12 was determined as indicated in METHODS. Data are means ± SE of 3 experiments.

(NATLDPRSFLLR) from the thrombin cleavage region on human PAR1, and by a monoclonal antibody (WEDE15) to the hirudin-like binding domain on human PAR1 (Fig. 7) (27). The wild-type $rPAR1_{EC}$ gave a doublet on immunoblot with anti-PAR1, SPAN12, and WEDE15 antibodies (Fig. 7, $rPAR1_{EC}$ lane). Also, the $rPAR1_{EC}$ fragment was recognized by a monoclonal antibody to the His tag present in the NH_2 terminus of the recombinant fusion protein (data not shown). The doublets of $rPAR1_{EC}$ seen on immunoblot in Fig. 7 represent some COOH-terminal proteolysis because the NH_2 terminal His tag was present on all wild-type and mutant forms of the recombinant protein.

When $rPAR1_{EC}$ was coupled to a microtiter plate, only goat anti-human PAR1 antibody raised to peptide NATLDPRSFLLR recognized the recombinant protein (data not shown). Polyclonal antisera to the analogous regions of human PAR3 or PAR4 did not recognize $rPAR1_{EC}$ linked to the microtiter plate cuvette wells (data not shown). Further specificity studies showed that when $rPAR1_{EC}$ was coupled to a microtiter plate, peptide RPPGF specifically bound to $rPAR1_{EC}$, as detected by a specific anti-RPPGF antibody followed by a secondary antibody (Fig. 8). These experiments indicate that immunochemically recognizable $rPAR1_{EC}$ was prepared and that it bound RPPGF. This interaction between RPPGF and $rPAR1_{EC}$ was specific for the entire peptide. L-Arg (5 mM), unlike RPPGF, did not block 50 μM biotin-RPPGF binding to $rPAR1_{EC}$ bound to microtiter plates (data not shown).

Investigations were then performed to determine the specific region on the $rPAR1_{EC}$ that bound RPPGF. Six recombinant deletion mutant forms of $rPAR1_{EC}$ were prepared by site-directed mutagenesis (Table 2). Five of these deletion mutants (*mutants I–V*) were missing two or four amino acids around the thrombin cleavage site on the $rPAR1_{EC}$. A sixth deletion mutant (*mutant VII*) was missing five amino acids at the hirudin-like binding region on PAR1 (Table 2). On immunoblot, polyclonal antibody to the peptide NATLDPRSFLLR was able to detect each of the mutagenized $rPAR1_{EC}$, although the wild-type protein and the deletion mutant of the hirudin-like binding region (*mutant VII*) were recognized better (Fig. 7). The monoclonal antibody SPAN12 only detected wild-type, *mutant V*, and *mutant VII* $rPAR1_{EC}$. Monoclonal antibody WEDE15 recognized all $rPAR1_{EC}$ except *mutant VII*, which had the deletion of amino acids YEPFW in the hirudin-like binding region (Table 2 and Fig. 7).

In competition-inhibition binding experiments, when $rPAR1_{EC}$ was coupled to a microtiter plate, soluble wild-type $rPAR1_{EC}$ inhibited biotin-RPPGF binding to linked $rPAR1_{EC}$ with an IC_{50} of 20 μM (Fig. 9). Deletion *mutant VII* of $rPAR1_{EC}$ of the hirudin-like

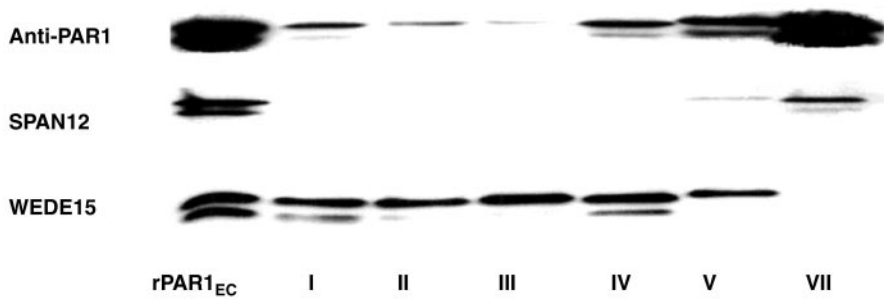

Fig. 7. Immunoblot studies on wild-type and deletion mutants of the recombinant extracellular domain of protease-activated receptor 1 ($rPAR1_{EC}$). Immunoreactivity of wild-type and various deletion mutants (*mutants I–V* and *VII*) of $rPAR1_{EC}$ to polyclonal goat anti-PAR1 antibody or monoclonal antibodies SPAN12 or WEDE15 was determined. One hundred nanograms of native and various deletion mutants of $rPAR1_{EC}$ were electrophoresed with 16.5% Tris-tricine SDS-PAGE and subsequently subjected to electroblot, followed by immunoblot with each of the listed antibodies. Various recognition patterns of each of these antibodies with wild-type and mutant forms of $rPAR1_{EC}$ are shown. The roman numerals shown under the immunoblot represent the specific mutant. Blots are representative of 2 experiments.

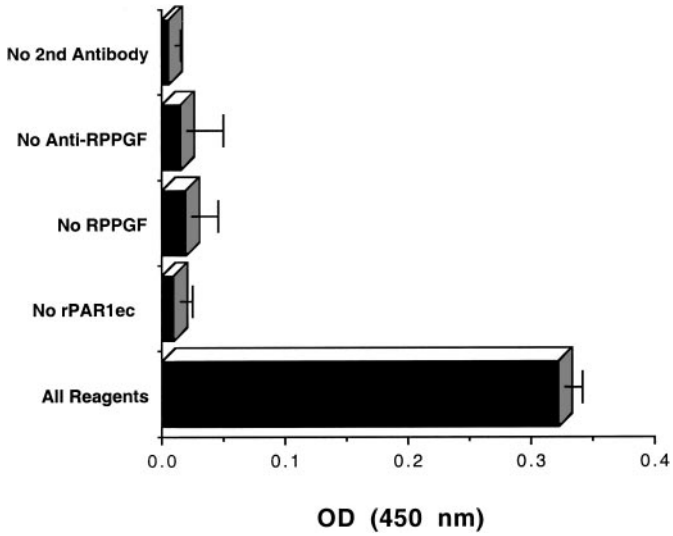

Fig. 8. Ability of RPPGF to bind to $rPAR1_{EC}$. $rPAR1_{EC}$ or bovine serum albumin (no $rPAR1_{EC}$), both at 1 μg/well in 0.1 M Na_2CO_3 (pH 9.6), was linked overnight at 4°C to microtiter plate cuvette wells. After being washed and blocked with 1% bovine serum albumin, wells were incubated with 1 mM RPPGF for 2 h at 37°C. At the end of the incubation, wells were washed and incubated with rabbit anti-RPPGF antibody (1:200) for 1 h at 37°C. Wells were then incubated with goat anti-rabbit antibody conjugated with horseradish peroxidase for 1 h at 37°C. In certain wells, no $rPAR1_{EC}$ was linked, no RPPGF was added, no anti-RPPGF was added, or the second antibody was excluded. The amount of secondary antibody bound to the primary antibody in the cuvette wells was determined as indicated in METHODS. Data are means ± SE of 3 experiments. This experiment indicates that RPPGF binds to linked $rPAR1_{EC}$ coupled to microtiter plates.

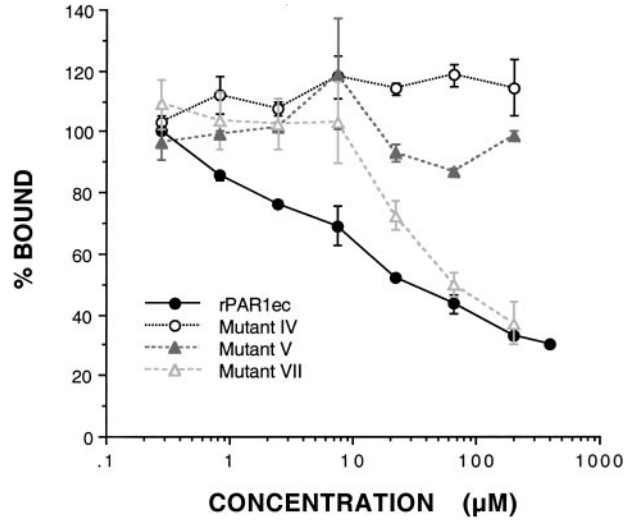

Fig. 9. Ability of wild-type or mutant $rPAR1_{EC}$ to compete biotin-RPPGF binding to immobilized $rPAR1_{EC}$. Wild-type $rPAR1_{EC}$ (1 μg/well) was linked to microtiter plate cuvette wells in 0.1 M Na_2CO_3 (pH 9.6) overnight at 4°C. After wells were washed and blocked with 1% bovine serum albumin, 10 μM biotin-RPPGF was added in the presence of increasing concentrations of wild-type, *mutant IV*, *mutant V*, or *mutant VII* $rPAR1_{EC}$ (0–400 μM; see Table 2 for characterization of the mutants). The amount of bound biotin-RPPGF was determined as indicated in METHODS. %Bound represents the percentage of the level of binding seen in the presence of a competitor versus that seen in the absence of the competitor. Data are means ± SE of 3 experiments.

binding site inhibited biotin-RPPGF binding to wild-type $rPAR1_{EC}$ with an IC_{50} = 65 μM (Fig. 9). Deletion *mutants I*, *II*, or *III*, which have amino acids LD, PR, or RS removed, respectively, also inhibited biotin-RPPGF binding to $rPAR1_{EC}$ (data not shown). However, deletion *mutant IV*, which had amino acids LDPR eliminated, or deletion *mutant V*, which had amino acids PRSF eliminated, did not block biotin-RPPGF binding to linked wild-type $rPAR1_{EC}$ (Fig. 9). These data indicate that RPPGF binding to $rPAR1_{EC}$ required the amino acids LDPR or PRSF to be present. Deletion *mutants I–III*, missing amino acids LD, PR, or RS, had a sufficient amount of structure present to compete with biotin-RPPGF binding to wild-type $rPAR1_{EC}$ like the natural sequence.

Ability of RPPGF and MAP4-RPPGF to inhibit thrombin's and thrombocytin's proteolysis of $rPAR1_{EC}$. Investigations were then performed to determine whether RPPGF and MAP4-RPPGF, a MAP form of RPPGF, blocked thrombin and thrombocytin proteolysis of PAR1. Thrombocytin is a thrombin-like snake venom enzyme that activates platelets by proteolysis of PAR1 (19, 22). Initial experiments determined whether RPPGF or MAP4-RPPGF prevented α-thrombin or thrombocytin proteolysis of wild-type $rPAR1_{EC}$ (Fig. 10). As the concentration of RPPGF increased from 0.125 to 1.0 mM, there was reduced thrombin proteolysis of $rPAR1_{EC}$ (Fig. 10*A*, *top*). In the presence of 1 mM RPPGF, 24% of $rPAR1_{EC}$ remained uncleaved by thrombin (Fig. 10*A*, *top*). When the thrombin-like enzyme thrombocytin was used, 0.5 and 1.0 mM RPPGF allowed for only 44% and 40% of $rPAR1_{EC}$ to be proteolyzed, respectively. More than 55% of $rPAR1_{EC}$ re-

Table 2. *Deletion mutants of the recombinant extracellular domain of PAR1*

Recombinant Protein	Sequence
Wild-type $rPAR1_{EC}$	A^{26}...N^{35}ATLDPR^{41}/S^{42}FLLRN...Y^{52}EPFWEDE^{60}E...S^{99}
Mutant I	A^{26}...N^{35}AT*LD*PR^{41}S^{42}FLLRN...Y^{52}EPFWEDE^{60}E...S^{99}
Mutant II	A^{26}...N^{35}ATLD*PR*^{41}/S^{42}FLLRN...Y^{52}EPFWEDE^{60}E...S^{99}
Mutant III	A^{26}...N^{35}ATLDP*R*^{41}/*S*^{42}FLLRN...Y^{52}EPFWEDE^{60}E...S^{99}
Mutant IV	A^{26}...N^{35}AT*LDPR*^{41}/S^{42}FLLRN...Y^{52}EPFWEDE^{60}E...S^{99}
Mutant V	A^{26}...N^{35}ATLD*PR*^{41}/*S*^{42}*F*LLRN...Y^{52}EPFWEDE^{60}E...S^{99}
Mutant VII	A^{26}...N^{35}ATLDPR^{41}/S^{42}FLLRN...*Y*^{52}*EPFW*EDE^{60}E...S^{99}

Wild-type $rPAR1_{EC}$ is a recombinant extracellular fragment of human protease-activated receptor 1 (PAR1) consisting of amino acid positions 26–99. The numbering is based on the sequence number of the amino acids in human PAR1 (28). The underlined and italicized letters represent the amino acids that were deleted from the extracellular domain of PAR1 by site-directed mutagenesis.

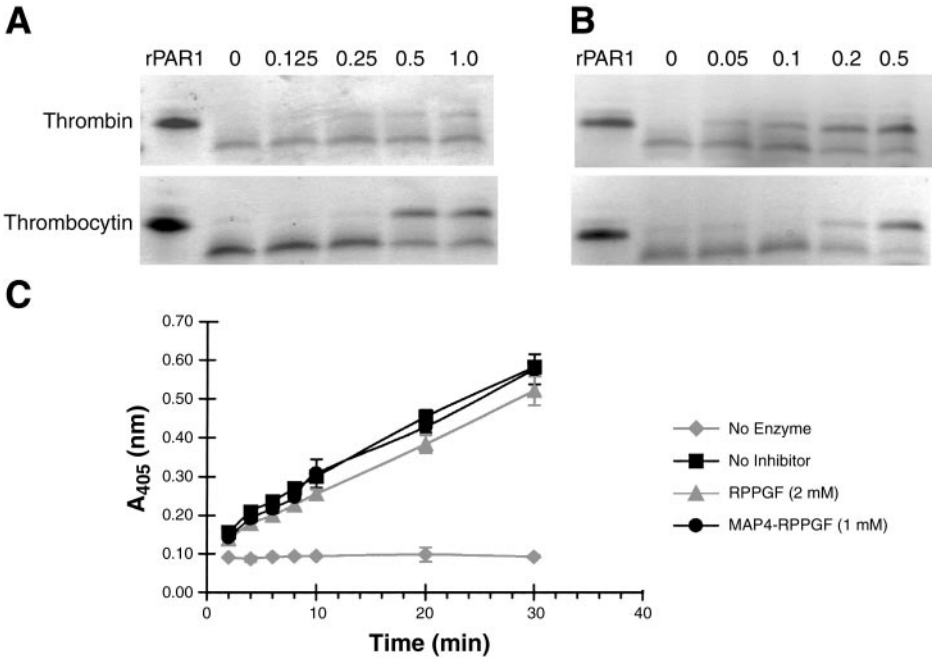

Fig. 10. Ability of RPPGF or the multiantigenic peptide form of RPPGF (MAP4-RPPGF) to inhibit thrombin or thrombocytin cleavage of $rPAR1_{EC}$. *A*: ability of RPPGF to inhibit the proteolytic cleavage of $rPAR1_{EC}$ by α-thrombin or thrombocytin. One microgram of $rPAR1_{EC}$ in 10 mM Tris·HCl and 200 mM NaCl (pH 8.0) was incubated at 37°C for 15 or 45 min with 1 nM α-thrombin or 0.5 μg/ml (16.7 nM) thrombocytin, respectively, in the absence or presence of increasing concentrations of RPPGF (0.125–1.0 nM). *B*: ability of MAP4-RPPGF to inhibit the proteolytic cleavage of $rPAR1_{EC}$ by α-thrombin or thrombocytin. $rPAR1_{EC}$ was treated with α-thrombin or thrombocytin as in *A* in the absence or presence of increasing concentrations of MAP4-RPPGF (0.05–0.5 mM). *C*: ability of thrombocytin (16.7 nM) to hydrolyze 1 mM H-D-Phe-Pip-Arg-paranitroanilide in the absence or presence of 2 mM RPPGF or 1 mM MAP4-RPPGF. Data are means ± SD of 3 replicates.

mained uncleaved (Fig. 10*A*, *bottom*). Additional studies were performed with a cluster peptide of RPPGF-MAP4-RPPGF. As the concentration of MAP4-RPPGF increased from 0.05 to 0.5 mM, there was reduced thrombin proteolysis of $rPAR1_{EC}$ (Fig. 10*A*, *top*). MAP4-RPPGF (0.2 and 0.5 mM) prevented thrombin from proteolyzing 78% and 82% of $rPAR1_{EC}$, respectively (Fig. 10*B*, *top*). Similarly, 0.5 mM MAP4-RPPGF allowed for only 24% cleavage of $rPAR1_{EC}$ by thrombocytin (Fig. 10*B*, *bottom*).

The concentrations of RPPGF and MAP4-RPPGF that prevented thrombin cleavage of $rPAR1_{EC}$ in Fig. 10, *A* and *B*, overlapped with those that prolonged the TCT (Fig. 1) (6). The prevention of cleavage data in Fig. 10 did not obviously confirm that these peptides blocked thrombin cleavage of $rPAR1_{EC}$ by binding to it. However, 2.0 mM RPPGF and 1.0 mM MAP4-RPPGF, concentrations twice that needed to prevent >50% cleavage of $rPAR1_{EC}$, did not directly inhibit 16.7 nM thrombocytin hydrolysis of the substrate H-D-Phe-Pip-Arg-paranitroanilide (Fig. 10*C*). These latter data indicate that the concentrations of RPPGF and MAP4-RPPGF used in the thrombocytin cleavage experiments (Fig. 10, *A* and *B*, *bottom*) could only have prevented the proteolysis of $rPAR1_{EC}$ by binding to the recombinant protein. These latter data, along with the experiments using deletion mutants of $rPAR1_{EC}$, indicated that RPPGF and related compounds also inhibit thrombin activation of platelets by binding to and preventing thrombin cleavage of PAR1 as a result of the bound peptide.

DISCUSSION

This study shows that RPPGF, an angiotensin-converting enzyme breakdown product of bradykinin, inhibits the ability of human α-thrombin to cleave PAR1 by both binding to the extracellular domain of human PAR1 near the thrombin cleavage site and by binding to the active site of α-thrombin itself. The affinity of RPPGF to bind to the extracellular domain of PAR1 is higher than its affinity to directly interact with the active site of thrombin. RPPGF blocks biotin-NATLD-PRSFLLR binding to linked RPPGC with an IC_{50} of 20 μM; $rPAR1_{EC}$ blocks biotin-RPPGF binding to linked $rPAR1_{EC}$ with an IC_{50} of 50 μM. Alternatively, RPPGF blocks α-thrombin's hydrolysis of Sar-Pro-Arg-pNA with a K_i of 1.75 mM. These findings explain the in vivo observation that RPPGF-induced platelet inhibition occurs at concentrations below that which inhibit the active site of thrombin (5, 6). Furthermore, it explains the observation that after infusions of RPPGF in dogs, there is a prolonged antiplatelet effect beyond the prolongation of the thrombin time and measurable plasma levels of the peptide (5, 6). Because RPPGF and MAP4-RPPGF do not inhibit the enzymatic activity of thrombocytin at the concentrations that inhibit thrombocytin proteolysis of PAR1, their major antiplatelet effect must be due to their ability to bind the extracellular domain of PAR1 to prevent proteolysis. These data suggest that inhibition of thrombin's active site and prevention of thrombin's ability to cleave PAR1, due to occupancy by RPPGF, could be occurring at the same time. This assessment is supported by the inability of two deletion mutants of $rPAR1_{EC}$ to inhibit RPPGF binding to wild-type recombinant protein. Finally, it is possible that RPPGF has a better ability to bind PAR1 in cell membranes than in solution to prevent thrombin cleavage. This finding might be why RPPGF appears to be a better platelet inhibitor in vivo (5, 6).

The finding that the NH_2-terminal portion of RPPGF (i.e., retrobinding) interacts directly with the active

site of α-thrombin was not expected. Crystal structures of thrombin complexed with retrobinding inhibitors are not very common. Only four such structures have been recognized: thrombin-BMS183507 (25), thrombin-nazumamide A (18), and thrombin-Sel 2711 or 2770 (13). These inhibitors have modified nonpeptide residues and are therefore different from RPPGF. Only the BMS183507 inhibitor forms a three hydrogen-bonded parallel β-sheet with Ser^{214}-Gly^{216}, whereas Sel 2711 and 2770 have two of the hydrogen bonds, and nazumamide A has none. Stabilization of the thrombin-nazumamide A complex appears to primarily come from interactions in the S1-S3 binding subsites of thrombin. The parallel β-strand interactions of RPPG are intermediate: two β-strands involve a poor hydrogen bonding angle (Table 1), whereas Pro^3 N does not have a hydrogen to make a hydrogen bond. The side chain interactions of BMS183507 and nazumamide A in the S1 pocket also are different than RPPGF and the selectide inhibitors. The former two have only one hydrogen bond in the salt bridge with Asp^{189} compared with doubly hydrogen-bonded salt bridges for others (Fig. 4). Moreover, only RPPGF has specific interactions with the catalytic triad of thrombin. It is the only retrobinder to the active site of α-thrombin with all naturally occurring amino acid residues. The interactions between thrombin and the RPPG peptide are largely through Arg^1-Pro^2, being overwhelmingly dominated by Arg^1 (Table 1). This fact is probably the reason for the relatively weak thrombin binding constant (K_i = 1.75 mM) of RPPGF to the active site of thrombin.

The experiments to determine whether there is a direct interaction between RPPGF and α-thrombin were begun by the observation that high concentrations of RPPGF influenced thrombin-mediated coagulant activity. The APTT, PT, and TCT are prolonged by high concentrations of RPPGF. The crystallization and kinetic experiments explain this observation. However, inhibition of the APTT and PT by RPPGF does not necessarily mean that these peptides are directly interfering only with thrombin. Recent studies indicate that RPPGF and MAP4-RPPGF interfere with thrombin activation of factor XI (6). In our animal investigations, the plasma concentration of RPPGF that inhibited coronary thrombosis was ≤8.7 μM, a value well below the minimal concentration of RPPGF that directly interacts with the active site of α-thrombin (5, 6). The present data indicate that RPPGF binds to the extracellular domain of PAR1 at amino acids LDPR or PRSF to prevent thrombin cleavage. This activity is probably the main mechanism by which RPPGF when infused into dogs interferes with thrombin activation of platelets in vivo.

There is little evidence to date that the interaction of RPPGF with the active site of thrombin is physiological. However, the native sequence of RPPGF may provide for a model compound to direct development efforts to prepare substrate-selective inhibitors of α-thrombin. RPPGF can be described as a substrate-directed thrombin inhibitor because it is partially directed to the thrombin substrate PAR1. Having compounds that separately inhibit the ability of α-thrombin to activate platelets without interacting with the active site of thrombin would be novel agents to examine for their clinical effect on arterial thrombosis. Selective thrombin inhibitors that interact with PAR1 to prevent thrombin cleavage may also be useful in regulating α-thrombin's mitogenic and inflammatory activities and the role of PAR1 in cancer cell metastasis.

This work was supported by National Heart, Lung, and Blood Institute Grants HL-56415 (to A. H. Schmaier), HL-43229 (to A. Tulinsky), HL-55907, HL-61081, and HL-61981 and by Michigan Economic Development Proposal 1607 (to A. A. K. Hasan).

Present address of A. A. K. Hasan: National Institutes of Health, National Heart, Lung, and Blood Institute, 6701 Rockledge Dr., MSC 7950, Bethesda, MD 20892-7950.

Present address of R. Krishnan: BioCryst Pharmaceuticals Incorporated, Birmingham, AL 35244.

REFERENCES

1. **Bode W, Turk D, and Karshikov AJ.** The refined 1.9 Å X-ray crystal structure of D-Phe-Pro-Arg-chloromethylketone inhibited human α-thrombin. *Protein Sci* 1: 426–471, 1992.
2. **Finzel BC.** Incorporation of fast Fourier transforms to speed restrained least-squares refinement of protein structures. *J Appl Crystallogr* 20: 53–55, 1987.
3. **Hasan AAK, Amenta S, and Schmaier AH.** Bradykinin and its metabolite, Arg-Pro-Pro-Gly-Phe, are selective inhibitors of α-thrombin-induced platelet activation. *Circulation* 94: 517–528, 1996.
4. **Hasan AAK, Cines DB, Zhang J, and Schmaier AH.** The C-terminus of bradykinin and N-terminus of the light chain of kininogens comprise an endothelial cell binding domain. *J Biol Chem* 269: 31822–31830, 1994.
5. **Hasan AAK, Rebello SS, Smith E, Srikanth S, Werns S, Driscoll E, Faul J, Brenner D, Normolle D, Lucchesi BR, and Schmaier AH.** Thrombostatin inhibits induced canine coronary thrombosis. *Thrombosis and Haemostasis* 82: 1182–1187, 1999.
6. **Hasan AAK, Schmaier AH, Warnock M, Normolle D, Driscoll E, Lucchesi BR, and Werns SW.** Thrombostatin inhibits cyclic flow variations in stenosed canine coronary arteries. *Thrombosis and Haemostasis* 86: 1296–1304, 2001.
7. **Higashi T.** Auto-indexing of oscillation images. *J Appl Crystallogr* 23: 253–257, 1990.
8. **Ishihara H, Connolly AJ, Zeng D, Kahn ML, Zheng YW, Timmons C, Tram T, and Coughlin SR.** Protease-activated receptor 3 is a second thrombin receptor in humans. *Nature* 386: 502–506, 1997.
9. **Krishnan R, Sadler JE, and Tulinsky A.** Structure of the Ser195Ala mutant of human α-thrombinb complexed with fibrinopeptide A(7–16): evidence for residual catalytic activity. *Acta Crystallogr D Crystallogr Biol* 56: 406–410, 2000.
10. **Krishnan R, Tulinsky A, Vlasuk GP, Pearson D, Vallar P, Bergum P, Brunck TK, and Ripka WC.** Synthesis, structure, and structure-activity relationships of divalent thrombin inhibitors containing an alpha-keto-amide transition-state mimetic. *Protein Sci* 5: 422–433, 1996.
11. **Majima M, Nishiyama K, Iguchi Y, Yao K, Ogino M, Ohno T, Sunahara N, Katoh K, Tatemichi N, Takei Y, and Katori M.** Determination of bradykinin-(1–5) in inflammatory exudate by anew ELISA as a reliable indicator of bradykinin generation. *Inflamm Res* 45: 416–423, 1996.
12. **Mathews JH, Krishnan R, Costanzo MJ, Maryanoff BE, and Tulinsky A.** Crystal structures of thrombin with thiazole-containing inhibitors: probes of the S1 binding site. *Biophysical J* 1: 2830–2839, 1996.
13. **Mochalkin I and Tulinsky A.** Structures of thrombin retro-inhibited with SEL2711 and SEL2770 as they relate to factor Xa. *Acta Crystallogr D Crystallogr Biol* 55: 785–793, 1999.

14. **Molino M, Blanchard N, Belmonte E, Tarver AP, Abrams C, Hoxie JA, Cerletti C, and Brass LF.** Proteolysis of the human platelet and endothelial cell thrombin receptor by neutrophil-derived cathepsin G. *J Biol Chem* 270: 11168–11175, 1995.
15. **Morinelli TA, Webb JG, Jaffa AA, Privitera PJ, and Margolius HS.** A metabolic fragment of bradykinin, Arg-Pro-Pro-Gly-Phe, protects against the deleterious effects of lipopolysaccharide in rats. *J Pharm Exp Thera* 296: 71–76, 2001.
16. **Murphey LJ, Hachey DL, Oates JA, Morrow JD, and Brown NJ.** Metabolism of bradykinin in vivo in humans: identification of BK1–5 as a stable plasma peptide metabolite. *J Pharm Exp Thera* 294: 263–269, 2000.
17. **Navaza J.** AMoRe:an automated package for molecular replacement. *Acta Crystallogr A* 50: 157–163, 1994.
18. **Nienaber VL and Amparo EC.** A noncleavable retro-binding peptide that spans the substrate binding cleft of serine proteases. Atomic structure of nazumamide A: human thrombin. *J Am Chem Soc* 118: 6807–6810, 1996.
19. **Niewiarowki S, Kirby EP, Brudzynski TM, and Stocker K.** Thrombocytin, a serine protease from *Bothrops atrox* venom. II. Interaction with platelets and plasma clotting factors. *Biochemistry* 18: 3570–3577, 1979.
20. **Prieto AR, Ma H, Huang R, Khan G, Schwartz KA, Hage-Korban EE, Schmaier AH, Hasan AAK, and Abela GS.** Thrombostatin, a metabolite of bradykinin, reduces platelet activation in a model of arterial wall injury. *Cardiovascular Research* 53: 984–992, 2002.
21. **Sack JS.** CHAIN-a crystallographic modeling program. *J Mol Graphic* 6: 244–245, 1988.
22. **Santos BF, Serrano SMT, Kuliopulos A, and Niewiarowski S.** Interaction of viper venom serine peptidases with thrombin receptors on human platelets. *FEBS Letters* 477: 199–202, 2000.
23. **Segal IH.** *Biochemical Calculations* (2nd ed.). New York: Wiley, 1976, p. 246–252.
24. **Skrzpczak-Jankun E, Carperas V, Ravichandran KG, Tulinsky A, Westbrook M, and Maraganore J.** Structure of the hirugen and hirulog complexes of α-thrombin. *J Mol Biol* 221: 1379–1393, 1991.
25. **Tabernero L, Chang CY, Ohringer SL, Lau WF, Iwanowicz EJ, Han WC, Wang TC, Seiler SM, Roberts DGM, and Sack JS.** Structure of a retro-binding peptide inhibitor complexed with human α-thrombin. *J Mol Biol* 246: 14–20, 1996.
26. **Tsiang M, Gibbs CS, Griffin LC, Dunn KE, and Leung LLK.** Selection of a suppressor mutation that restores affinity of an oligonucleotide inhibitor for thrombin using in vitro genetics. *J Biol Chem* 270: 19370–19376, 1995.
27. **Vu TKH, Hung DT, Wheaton VI, and Coughlin SR.** Molecular cloning of a functional thrombin receptor reveals a novel proteolytic mechanism of receptor activation. *Cell* 64: 1057–1068, 1991.
28. **Xu WF, Andersen H, Whitmore TE, Presnell SR, Yee DP, Ching A, Gilbert T, Davie EW, and Foster DC.** Cloning and characterization of human protease-activated receptor 4. *Proc Natl Acad Sci* 95: 6642–6646, 1998.